UCRL-JRNL-233134

Atomic Models for Motional Stark Effects Diagnostics

M. F. Gu, C. Holcomb, J. Jayakuma, S. Allen, N. A. Pablant, K. Burrell

July 27, 2007

Disclaimer

This document was prepared as an account of work sponsored by an agency of the United States Government. Neither the United States Government nor the University of California nor any of their employees, makes any warranty, express or implied, or assumes any legal liability or responsibility for the accuracy, completeness, or usefulness of any information, apparatus, product, or process disclosed, or represents that its use would not infringe privately owned rights. Reference herein to any specific commercial product, process, or service by trade name, trademark, manufacturer, or otherwise, does not necessarily constitute or imply its endorsement, recommendation, or favoring by the United States Government or the University of California. The views and opinions of authors expressed herein do not necessarily state or reflect those of the United States Government or the University of California, and shall not be used for advertising or product endorsement purposes.

Atomic Models for Motional Stark Effects Diagnostics

M. F. Gu†, C. Holcomb†, J. Jayakuma†, S. Allen†, N. A. Pablant‡, and K. Burrell§

† Lawrence Livermore National Laboratory, Livermore, CA 94550, USA
‡ University of California San Diego, La Jolla, CA 92037, USA
§ General Atomics, La Jolla, CA 92037, USA

Abstract. We present detailed atomic physics models for motional Stark effects (MSE) diagnostic on magnetic fusion devices. Excitation and ionization cross sections of the hydrogen or deuterium beam traveling in a magnetic field in collisions with electrons, ions, and neutral gas are calculated in the first Born approximation. The density matrices and polarization states of individual Stark-Zeeman components of the Balmer α line are obtained for both beam into plasma and beam into gas models. A detailed comparison of the model calculations and the MSE polarimetry and spectral intensity measurements obtained at the DIII-D tokamak is carried out. Although our beam into gas models provide a qualitative explanation for the larger π/σ intensity ratios and represent significant improvements over the statistical population models, empirical adjustment factors ranging from 1.0–2.0 must still be applied to individual line intensities to bring the calculations into full agreement with the observations. Nevertheless, we demonstrate that beam into gas measurements can be used successfully as calibration procedures for measuring the magnetic pitch angle through π/σ intensity ratios. The analyses of the filter-scan polarization spectra from the DIII-D MSE polarimetry system indicate unknown channel and time dependent light contaminations in the beam into gas measurements. Such contaminations may be the main reason for the failure of beam into gas calibration on MSE polarimetry systems.

1. Introduction

This paper discusses a new, predictive model of the Balmer α spectrum in the presence of a motional Stark electric field that has direct application to tokamak fusion energy research. The strong electric field causes the Balmer α line to split into nine principal components with distinct polarization properties. Six of them, $\pi_{\pm 2}$, $\pi_{\pm 3}$, and $\pi_{\pm 4}$ components, are polarized along the electric field direction, and the remaining three, σ_0, $\sigma_{\pm 1}$ are polarized perpendicular to the electric field. The Zeeman splitting caused by the magnetic field is much smaller than the Stark effects, and is generally neglected in typical tokamak applications. The Motional Stark Effect diagnostic (MSE) makes polarimetric measurements of Deuterium emission from a neutral beam injected into a magnetized tokamak plasma (Levinton et al., 1989; Wróblewski et al., 1990). The polarization of

either the π or σ components may be used to determine the pitch of the helical magnetic field as a function of radius, which is a key parameter affecting tokamak performance. The required measurement accuracy demands a reliable calibration procedure. In general, there are a large number of parameters that can affect the calibration of an MSE diagnostic over time, including multiple fold mirrors, Faraday rotation in refractive optics, and coatings, induced stresses, and erosion caused by interaction of components with plasma. In-situ calibration techniques are needed to cope with these issues. Firing the neutral beam into a gas may be an attractive way to produce a fiducial Stark-split Balmer α spectrum in a vacuum magnetic field. Actual use of beam into gas for calibration on existing tokamaks has not yet been proved to be accurate enough. In particular, on the DIII-D tokamak (San Diego, USA), beam into gas is usually run at 0.5 mTorr in a 37 m^3 tank (at a density of 1.6×10^{13}cm^{-3}). Among the observed complications is a total π intensity that exceeds the σ intensity by roughly a factor of two compared to the beam into plasma condition.

One particular concern in modeling the Stark spectrum of the Balmer α line is whether the upper state populations achieve statistical distribution in either beam into plasma or beam into gas measurements. The observed intensity ratios of π and σ components in beam into plasma case are often consistent with the assumption of statistical equilibrium at typical tokamak plasma densities above a few $\times 10^{13}$ cm^{-3}. The beam into gas measurements, however, indicate that this assumption is questionable. With non-statistical populations in the upper states, the intensity ratios depend on a multitude of collisional processes, and detailed knowledge of their cross sections are needed to obtain a reliable spectral model. A further complication arises because Stark components are split into several features by the magnetic field, and individual Stark-Zeeman lines have different polarization properties from the Stark component as a whole. Such differences may manifest themselves in the polarization spectrum even if the instrument cannot resolve individual components.

In this paper, we present detailed atomic physics modeling of the Stark-Zeeman Spectrum of the deuterium Balmer α lines for both beam into plasma and gas measurements. We calculate excitation and ionization cross sections of the deuterium atom in collision with charged particles and neutral gas using a first order Born approximation. The effects of charge exchange processes between deuterium ions and the neutral gas are also investigated using theoretical electron capture cross sections calculated in the continuum distorted-wave approximation. In §2, we discuss the details of our atomic model, and compare the collisional and radiative data in the present work with previous publications wherever available. §3 presents the collisional radiative model calculations for both beam into plasma and beam into gas measurements. In §4, we calculate the polarization properties of individual Stark-Zeeman components using the density matrix formalism and compare the results with simple geometric predictions. A detailed comparison of our models and experiments at DIII-D tokamak is given in §5. §6 gives a brief summary of the present results.

2. Atomic Data for Hydrogen in External Fields

The dependence of energy levels and radiative transition rates of the hydrogen atom on the external electric and magnetic fields is well studied (Foley & Levinton, 2006; Mandl et al., 1993). In the present work, we solve the Dirac equation for the hydrogen atom with a field-dependent Hamiltonian

$$
\begin{aligned}
H &= H_0 + H_B^{(1)} + H_B^{(2)} + H_E \\
H_B^{(1)} &= \mu_B \left(2\vec{S} + \vec{L} \right) \cdot \vec{B} \\
H_B^{(2)} &= \frac{1}{2} \mu_B^2 \left| \vec{B} \times \vec{r} \right|^2 \\
H_E &= e\vec{E} \cdot \vec{r},
\end{aligned}
\tag{1}
$$

where H_0 is the field-free Dirac Hamiltonian, $H_B^{(1)}$ is the linear Zeeman term, $H_B^{(2)}$ is the diamagnetic Zeeman term, H_E is the interaction with the electric field, $\vec{S}$, $\vec{L}$, and $\vec{r}$, are the spin angular momentum, orbital angular momentum, and position operators of the electron, $\mu_B = 5.788 \times 10^{-5}$ eV T^{-1} is the Bohr magneton, and $\vec{E}$ and $\vec{B}$ are the electric and magnetic field vectors. The wavefunction of the system is assumed to be $\psi = \sum_i b_i \phi_i$, where ϕ_i is the field free eigenfunction of H_0, and b_i are mixing coefficients. For the field strengths relevant in magnetic fusion devices, only levels with the same principal quantum number, n, mix significantly, and the total Hamiltonian matrix is block diagonal in the ϕ_i basis set with each block having dimension $2n^2$. The diagonalization of these block matrices results in eigenenergies and mixing coefficients for individual Stark-Zeeman levels. Once wavefunctions are known, it is straightforward to calculate the radiative transition rates between Stark-Zeeman levels. As an example, in Figure 1 and 2, we show the energy splittings of $n = 2$ Stark-Zeeman levels and the radiative transition rates of these levels to the $n = 1$ states, for magnetic field strengths between 5 and 5×10^4 G, and an orthogonal electric field of $2.4 \left(\frac{B}{1G} \right)$ V cm^{-1}, which is generated by the motional Stark effect of a 30 keV hydrogen beam traveling in a direction perpendicular to the magnetic field. The results obtained here agree with those of Foley & Levinton (2006) for the common range of field strength values.

In order to model the MSE spectrum of the Balmer α lines in situations where the upper level populations are not in statistical distribution, one needs detailed knowledge of cross sections of various collisional processes connecting individual Stark-Zeeman levels. For beam into plasma measurements, the relevant processes include collisional excitation and ionization of beam neutrals by electrons and plasma ions and charge exchange between plasma ions and beam neutrals. The radiative recombination between beam ions and electrons is generally negligible due to their small cross sections. For beam into gas measurements, one must consider excitation and ionization of beam neutrals in collisions with the background gas and charge exchange between beam ions and the gas. In the modeling of Balmer α spectrum of deuterium in the JET plasma, Boileau et al. (1989) used the first Born approximation to calculate various excitation and ionization cross sections of the beam neutrals by electron and plasma ion collisions.
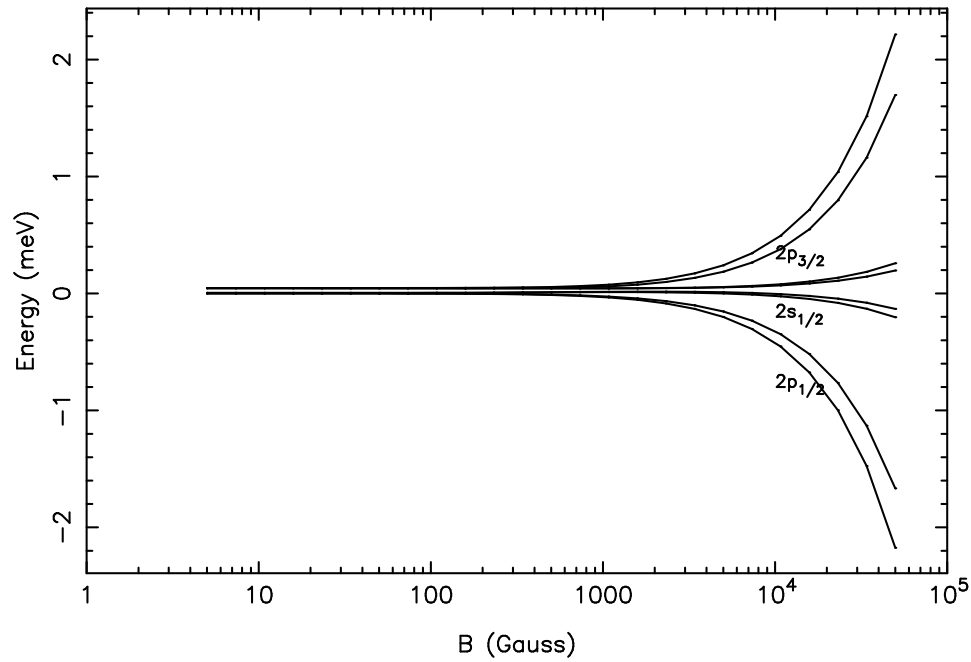
Figure 1. Energy splittings of $n = 2$ states of hydrogen in the magnetic and motional Stark fields for a beam energy of 30 keV and beam direction perpendicular to the magnetic field.
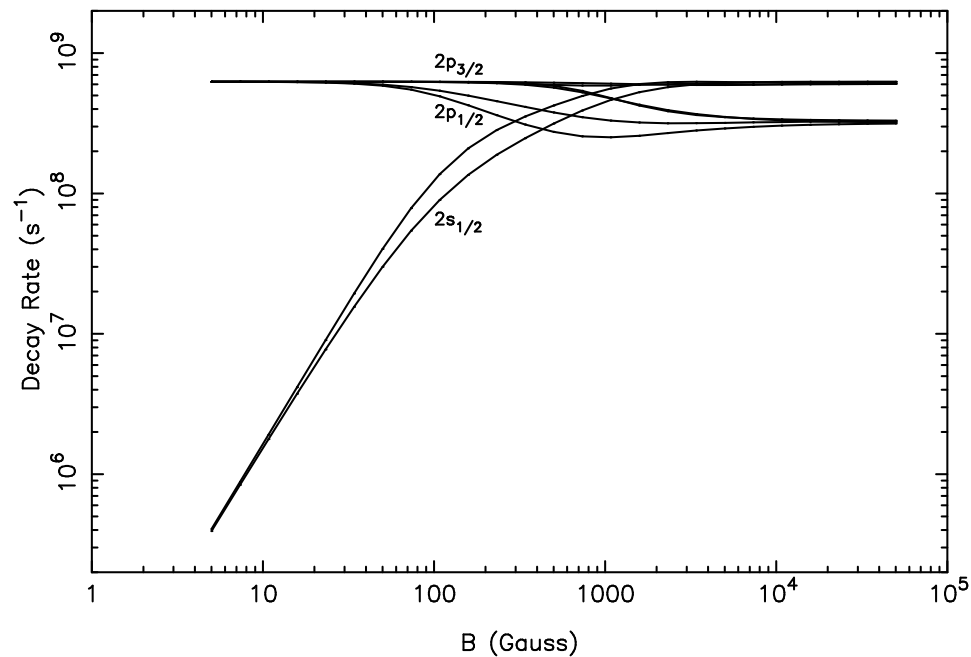

Figure 2. Radiative transition rates of $n = 2$ states of hydrogen to $n = 1$ states in the magnetic and motional Stark fields for a beam energy of 30 keV and beam direction perpendicular to the magnetic field.

The resulting simulated spectra were found to agree with the measurements to within 50%. Foley & Levinton (2006) constructed a collisional radiative model for the beam into gas measurements, and cross sections for charge exchange, excitation and ionization were taken from experimentally determined values in the literature whenever available. However, these experimental values are obtained in the field-free environments, and do not take into account Stark-Zeeman splitting. Moreover, the availability of such experimental cross sections are quite limited. The vast amount of cross sections for collisional mixing of sublevels do not exist. In the present work, we have implemented the first Born approximation for collisional excitation and ionization of the hydrogen or deuterium beam by collisions with electrons, ions, and neutral atoms. The first Born theory, or the so-called Bethe theory, of inelastic collisions between atoms and fast charged particles has been reviewed by Inokuti (1971), and the analogous theory for atom-atom collisions has been described by Levy II (1969) and Gillespie & Inokuti (1980). The main difference between the atom-ion and atom-atom collisions is the need to take into account the electronic screening in the target neutral for the latter.The significant modification to these descriptions in the present work involves the use of wavefunctions of individual Stark-Zeeman levels instead of zero-field wavefunctions.

To validate the present implementation of the first Born theory of electron-atom and ion-atom collisions, we calculated the electron and proton collisional excitation cross sections of the hydrogen atom between the $1s$ and $n = 3$ states in the absence of external fields, and compared the results with the calculations of Boileau et al. (1989), and the experimental measurements of Park et al. (1976) in Figure 3. It is seen that our results agree with Boileau et al. (1989) to within 20%, and that the first Born approximation is valid for collision energies above 40 keV for a hydrogen beam, or 80 keV for a deuterium beam.

We have also investigated the validity of the atom-atom cross sections of the present work through comparisons with various experimental measurements. In Figure 4, we show the calculated excitation cross sections of H($1s$)→H(nl) in collisions with H_2 gas and electrons, and the comparison with experimental cross sections of H-H_2 collisions. The H_2 molecule is treated as two individual H atoms in our calculations for simplicity. It is clear that electron collisional excitation cross sections are generally a factor few to ten larger than the neutral gas excitation cross sections. The agreements between the calculated and measured cross sections for H-H_2 collisions are generally within a factor two, except for excitation to $3p$, where differences of a factor of 6 are seen. However, the measurements exist only for collision energies below 40 keV, where first Born approximation is expected to start breaking down.

Figure 5 shows the cross sections of H($2s$) in collision with the H_2 gas. Because experimental cross sections exist only for excitation to $3s$, the total production of Ly_α and Balmer α lines, and electron loss, the corresponding theoretical values are obtained by summing various contributions. The discrepancies between the measured and calculated values are seen to be within a factor of few, although the measurements exist only for collision energies below 30 keV, where first Born approximation is less
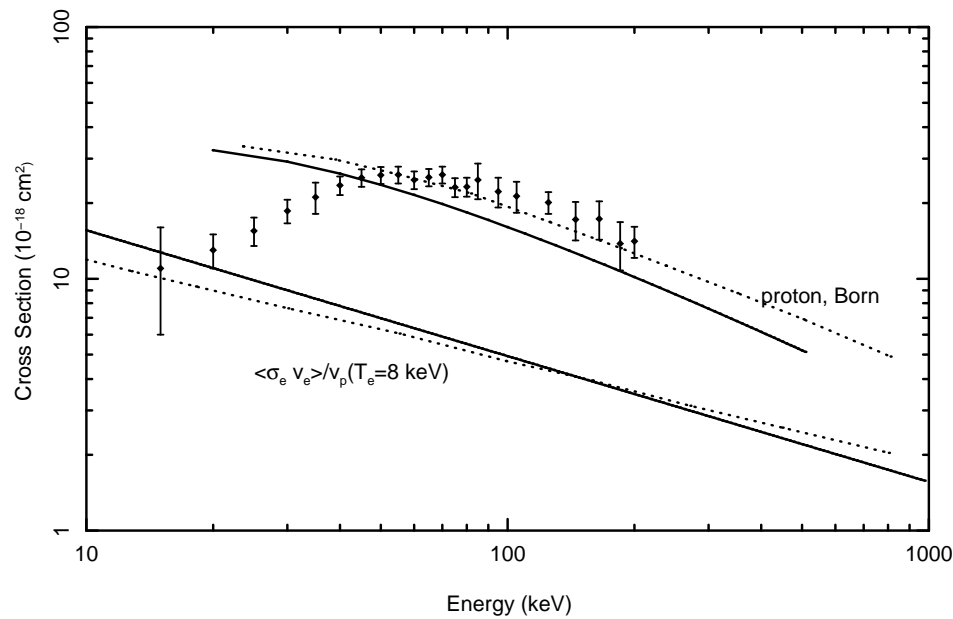
Figure 3. Comparison of electron and proton impact excitation cross sections for H($1s$)→H($n = 3$). Solid lines are the present results, dotted lines are from Boileau et al. (1989), and filled circles with error bars are experimental cross sections for proton excitation from Park et al. (1976).
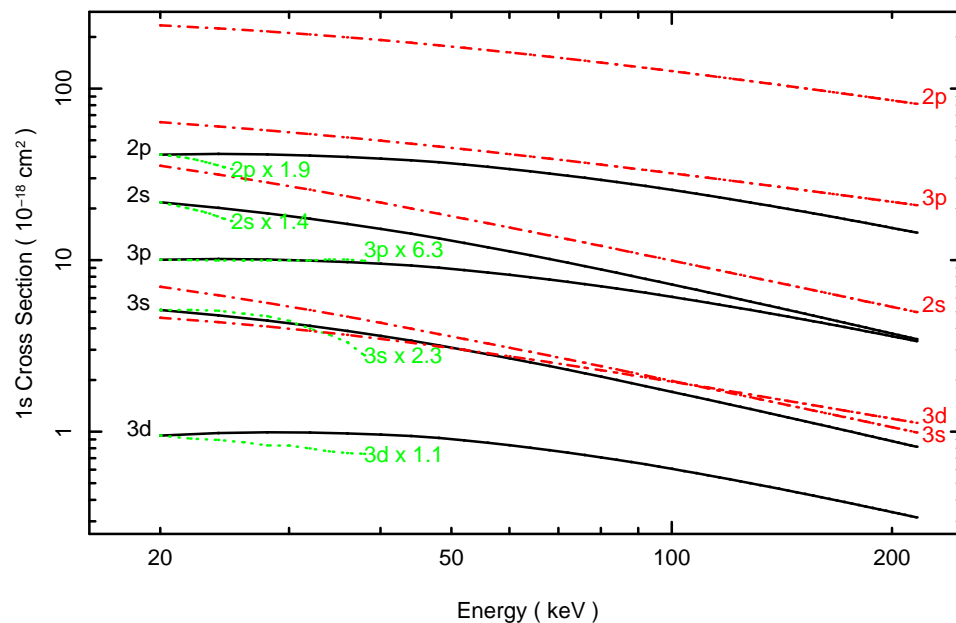

Figure 4. Comparison of collisional excitation cross sections for H($1s$)→H($2l,3l$) in collision with electron and H_2 gas. The solid black lines are for H-H_2 collision, the red dot-dashed lines are for H-e collision, and the green dotted lines are the measured H-H_2 cross sections taken from Hughes et al. (1972) and multiplied by the factor indicated in the figure.
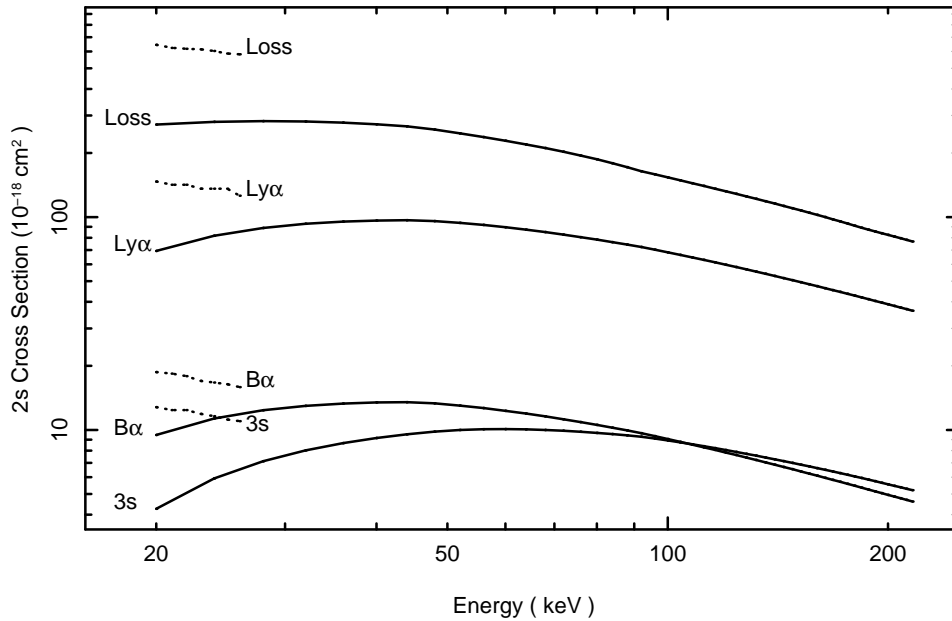
Figure 5. Comparison of cross sections of H($2s$)-H$_2$ collisions. The solid lines are the present calculations, dotted lines are the experimental measurements of McKee et al. (1979) and Hill et al. (1980).

reliable.

Geddes et al. (1987) measured the total collisional destruction cross section of H($3s$) in H$_2$, including excitation and electron loss processes. The comparison of the measured and calculated values is shown in Figure6. The discrepancies between the two are seen to within a factor of few.

The charge exchange cross sections between beam neutrals and plasma ions in the beam into plasma measurements, and beam ions and background gas in the beam into gas measurements are determined using the continuum-distorted-wave approximation implemented in Belkić et al. (1984). This program calculates cross sections without external fields. We approximate the charge exchange cross sections for individual Stark-Zeeman levels, ψ, as

$$\sigma(\psi) = \sum_i b_i^2 \sigma(\phi_i), \tag{2}$$

i.e., the cross sections obtained with zero-field basis wavefunctions are weighted by the square of mixing coefficients.

3. Collisional Radiative Models For Beam into Plasma and Gas Measurements

A collisional radiative model for a deuterium beam is constructed using the atomic data discussed in the previous section. All $n \leq 4$ levels are resolved into Stark-Zeeman components, while those with $4 < n \leq 10$ are included as zero-field fine-structure levels to approximate the cascade contributions to the Balmer α lines. The rates for collisional
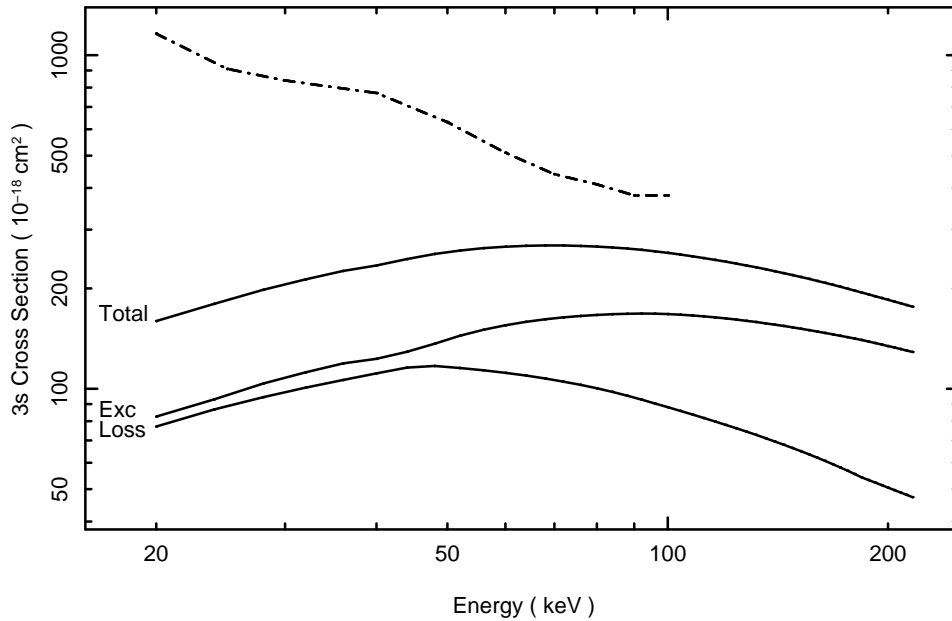
Figure 6. Comparison of total collisional destruction cross sections of H($3s$) in H$_2$. The solid lines are the present calculations, the dot-dashed lines are the measurements of Geddes et al. (1987).

and radiative processes connecting the Stark-Zeeman levels with $n \leq 4$ and the zero-field states with $n > 4$ are determined the same way as obtaining charge exchange cross sections by weighting the field-free values with the square of mixing coefficients. The collisional deexcitation cross sections are obtained from the excitation cross sections with the relation of detailed balance.

For both beam into plasma and gas measurements, we construct two classes of models. One does not take into account ionization and charge exchange recombination processes leading to beam attenuation, the other includes full effects of ionization and recombination, and track both neutral and ionized deuterium density of the beam. Upon injection, the beam is assumed to be neutral initially, and the two Stark-Zeeman components of the $n = 1$ states are equally populated with no excited states population.

For beam into plasma models, the plasma is assumed to be comprised of electrons and deuterons with equal density and having a temperature of 4 keV. One can in principle include effects of impurity ions by adopting an effective charge, Z_{eff}, in the calculation of ion-atom cross sections. However, taking $Z_{eff} = 1$ appears to be a good approximation for the DIII-D tokamak plasma as demonstrated in §5.

We carried out calculations for a deuterium beam of 80 keV traveling in a direction that makes an angle of 60° with the magnetic field direction. The results presented below are all calculated for a magnetic field strength of 2.1 T, which is typical for DIII-D plasma shots. The plasma and gas densities range from 10^5 to 10^{17} cm^{-3} in our models. In Figure 7, we show the populations of $n = 2$, 3, and 4 Stark-Zeeman states along the beam line for the beam into plasma model without ionization and charge exchange recombination processes at several plasma densities. Figure 8 shows the

population evolution for the beam into plasma model with ionization and recombination processes. The statistical equilibrium for the states within the manifold of a given principal quantum number is achieved when all sublevels become equally populated. It is clear that the statistical distribution of $n = 3$ states is obtained approximately at plasma densities of $\sim 10^{14}$ cm^{-3}, and there are significant beam attenuation effects at such densities due to ionization and charge exchange of the beam neutrals.

The population evolution for beam into gas models without and with ionization and charge exchange processes are shown in Figure 9 and 10, respectively, for several densities. They illustrate that the populations of $n = 3$ states do not achieve statistical distribution until the density reaches 10^{16} cm^{-3} when ionization and charge exchange processes are not included. With ionization and charge exchange processes, the populations do not reach statistical distribution even at very high densities, which reflects the fact that there is no detailed balance between charge exchange recombination of the beam ions and ionization of the beam neutrals. In typical beam into gas measurements at tokamak devices such as DIII-D, the gas density is $\sim 10^{13}$ cm^{-3}. At such low densities, the effects of ionization and charge exchange are not significant. The lack of statistical distribution among the $n = 3$ levels has important implications for the intensity ratios and polarization properties of the Balmer α Stark-Zeeman spectrum.

4. Intensities and Polarizations of Balmer α Lines

The intensity ratios and polarization angles of π and σ components have long been used as diagnostics of magnetic field strength and direction in tokamak devices. However, proper calibration of instruments is essential for reliable measurements. Beam into gas measurements have been proposed as a potential calibration procedure, as it closely recreates the experimental configuration of the actual beam into plasma application. However, as the results in the previous section indicate, the Balmer α upper level populations are in statistical distribution for typical tokamak plasma densities of $> 5 \times 10^{13}$ cm^{-3}, which is generally not the case for beam into gas measurements. Therefore, it is important to understand the intensities and polarization properties of individual Stark-Zeeman components.

The polarization state of a photon is most conveniently described by its density matrix in the helicity representation (Steffen & Alder, 1975)

$$\rho = \frac{I}{2}\left(1 - \frac{Q}{I}\sigma_x - \frac{U}{I}\sigma_y + \frac{V}{I}\sigma_z\right), \tag{3}$$

where σ_x, σ_y, and σ_z are Pauli matrices, and I, Q, U, and V are known as the Stokes parameters. The density matrix of an electric dipole transition, as is the case for Balmer α photons, are calculated as

$$< \tau|\rho|\tau' > \ = \frac{d\Omega}{4\pi}(\alpha\omega)^3 \sum_{\lambda q} C_q^\lambda(\tau,\tau') D_{q,\tau'-\tau}^{\lambda*}(\hat{e}_z \to \hat{k})$$

$$C_q^\lambda(\tau,\tau') \ = C \sum_{MM'} (-1)^{M'-\tau'} < \psi_i|E_M^1|\psi_f > < \psi_f|E_{M'}^1|\psi_i >$$
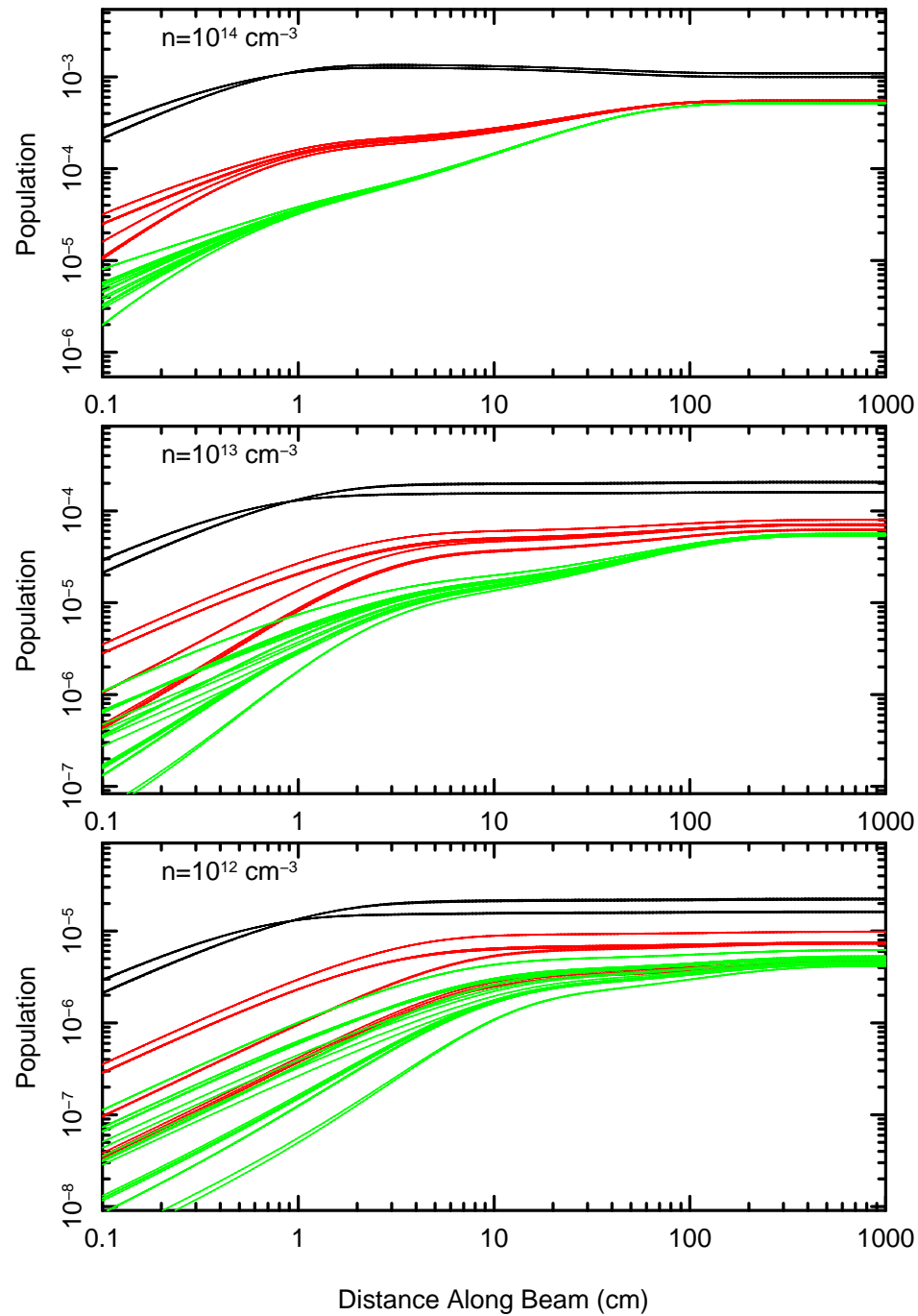
Figure 7. Population evolution of the $n = 2$ (black), 3 (red), and 4 (green) levels for a deuterium beam into plasma model without ionization and charge exchange processes. Statistical equilibrium for a given n-manifold is achieved when all sublevels have equal populations.
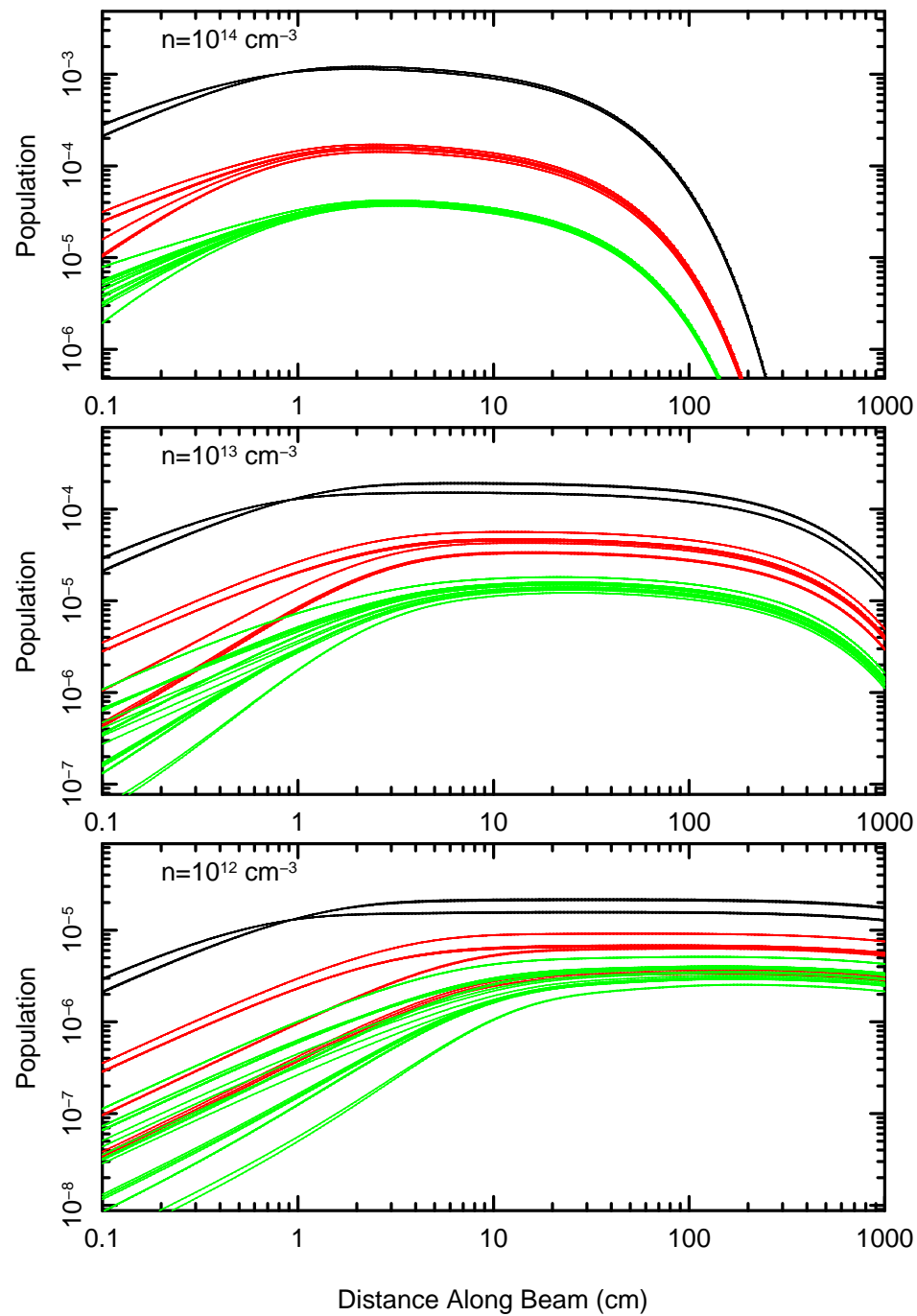
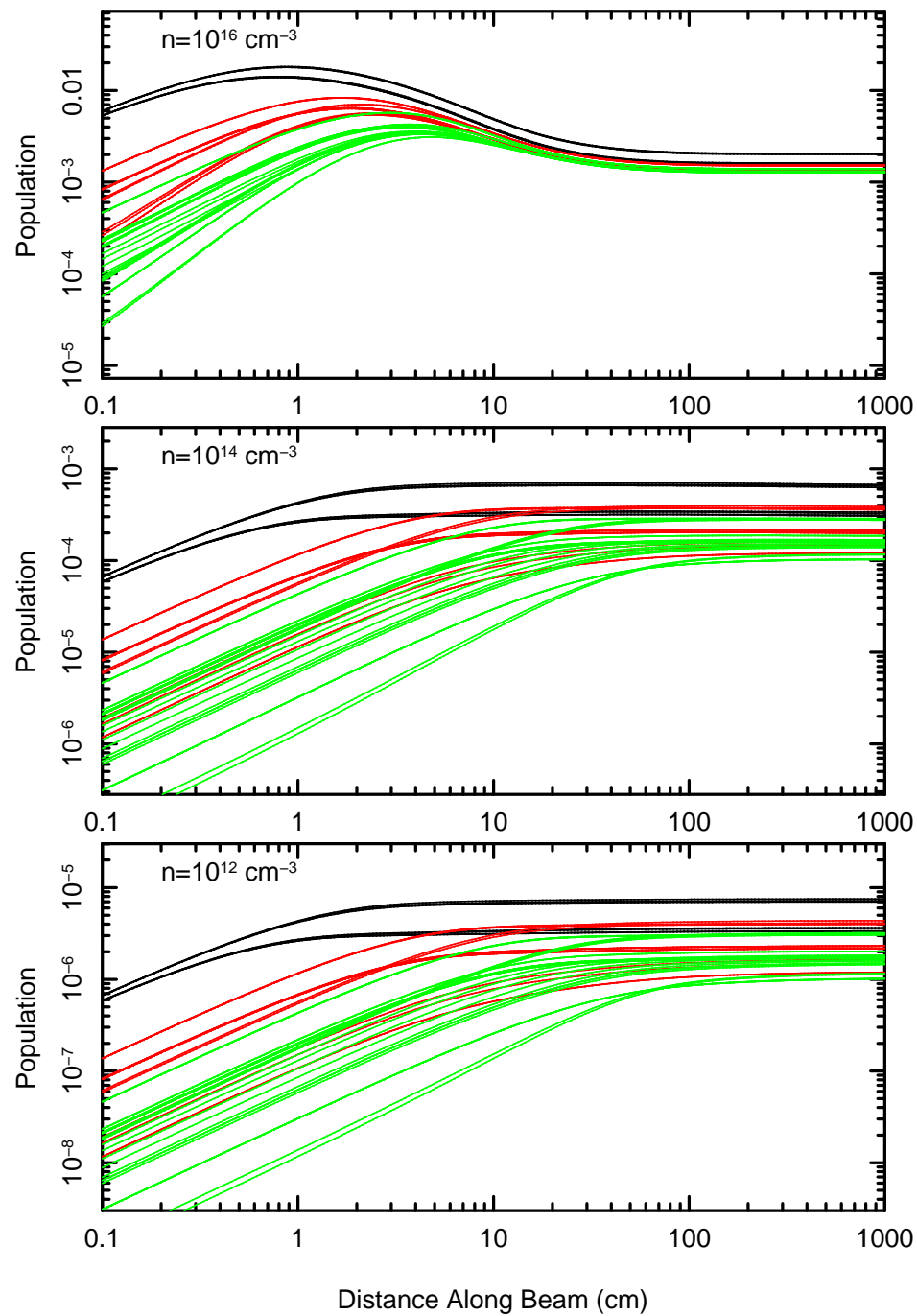**Figure 8.** Same as Figure 7, but for beam into plasma model with ionization and charge exchange processes.

Figure 9. Same as Figure 7, but for beam into gas model without ionization and charge exchange processes.
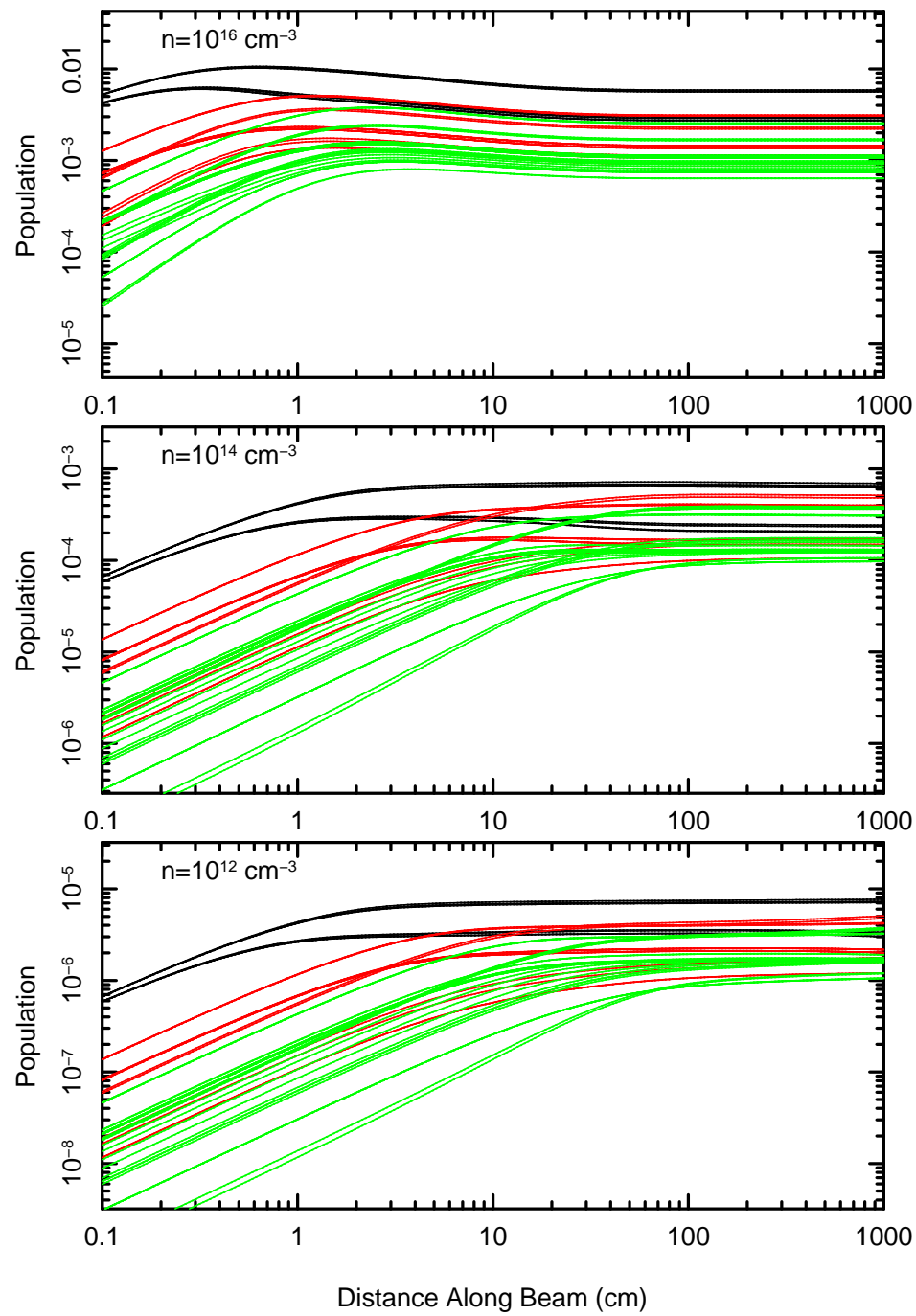
Figure 10. Same as Figure 7, but for beam into gas model with ionization and charge exchange processes.

Table 1. Stokes parameters of π and σ components for beam into plasma and gas models at a density of 10^{14} cm^{-3}.

		π_{-4}	π_{-3}	π_{-2}	σ_{-1}	σ_0	σ_1	π_2	π_3	π_4
	plasma	31.567	42.413	13.507	35.538	99.720	35.585	13.724	41.992	31.241
I	gas	23.214	12.141	10.724	9.872	27.742	9.967	10.899	12.040	23.177
	plasma	0.990	0.994	0.967	-0.992	-1.000	-0.993	0.967	0.994	0.991
Q/I	gas	0.990	0.994	0.991	-0.991	-1.000	-0.993	0.992	0.995	0.991
	plasma	0.000	0.000	0.000	0.000	0.000	0.000	0.000	0.000	0.000
U/I	gas	0.000	0.000	0.000	0.000	0.000	0.000	0.000	0.000	0.000
	plasma	-0.138	-0.070	-0.023	-0.061	0.002	0.057	0.014	0.075	0.135
V/I	gas	-0.138	-0.068	0.005	-0.067	0.005	0.062	-0.017	0.073	0.135

$$\times\ (2\lambda + 1) \begin{pmatrix} 1 & 1 & \lambda \\ M & -M' & q \end{pmatrix} \begin{pmatrix} 1 & 1 & \lambda \\ \tau & -\tau' & \tau' - \tau \end{pmatrix}, \tag{4}$$

where τ and τ' represent the helicity states of the photon, $\hat{e}_z$ is the Z-axis of the coordinate system in which the atomic states are quantized, $\hat{k}$ is the direction of the photon propagation, α is the fine structure constant, ω is the transition energy in atomic units, $d\Omega$ is the solid angle differential element around $\hat{k}$, ψ_i and ψ_f are the initial and final atomic states, E_M^1 is the spherical tensor component of the electric dipole operator, and $\begin{pmatrix} j_1 & j_2 & j_3 \\ m_1 & m_2 & m_3 \end{pmatrix}$ represents the Wigner $3j$ symbol. The normalization constant C is chosen to ensure that after integrating over $d\Omega$ and summing over the diagonal elements, one obtains the total radiative decay rate from state ψ_i to ψ_f. The Wigner D-Matrix, $D_{q,u}^{\lambda*}$, is defined as

$$D_{q,u}^{\lambda*}(\alpha, \beta, \gamma) = <\lambda q|e^{-iJ_z\alpha}e^{-iJ_y\beta}e^{-iJ_z\gamma}|\lambda u>, \tag{5}$$

where J_y and J_z are angular momentum operators, $|\lambda q>$ is the angular momentum eigenstate, α, β, and γ are the Euler angles corresponding to the coordinate transformation from $\hat{e}_z$ to $\hat{k}$. The angular distribution of the radiation field is completely specified by the Wigner D-Matrix. If a spectral feature is comprised of multiple Stark-Zeeman components, one obtains the density matrix, or Stokes parameters, by weighting the density matrices of individual components with the upper level populations.

For any given field geometry and view direction, it is straightforward to calculate Stokes parameters and intensities of Balmer α components from the density matrices. As an example, Table 1 shows the Stokes parameters of σ and π components of the Balmer α line for the beam into plasma and gas models at a density of 10^{14} cm^{-3}. The view direction, $\hat{k}$, is in the $\vec{v}$-$\vec{B}$ plane, where $\vec{v}$ is the beam velocity. The angle between $\hat{k}$ and $\vec{B}$ is 60°, and that between $\hat{k}$ and $\vec{v}$ is 120°. It is seen that by summing over individual sub-components of σ and π lines, one recovers their nearly pure linear polarization states. The small circular polarization fractions are caused by the Zeeman effects. The differences in the polarization states and intensity ratios between beam into plasma and gas models are caused by the non-statistical distribution of the upper levels in the beam into gas case. In Figure 11, we show the relative intensities of σ and π components as functions of plasma densities for beam into plasma models with
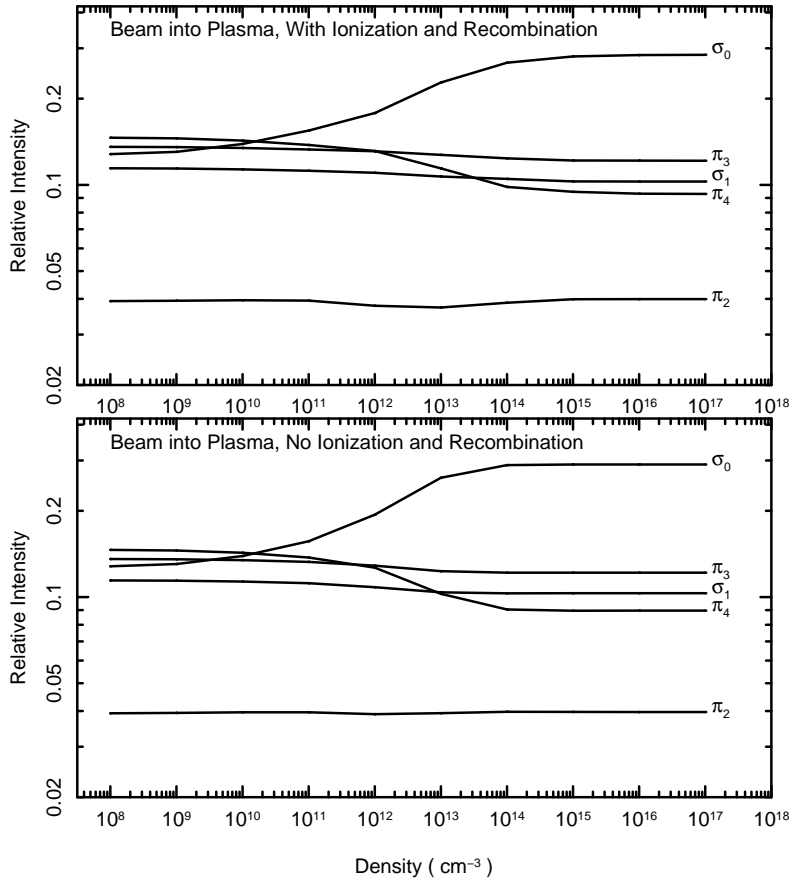
Figure 11. Relative intensities of σ and π components as functions of plasma density for beam into plasma models.

and without ionization and charge exchange processes. Figure 12 shows the relative intensities for the beam into gas models. The effects of non-statistical distribution of the upper levels are more clearly seen in these figures.

The primary goal of the MSE diagnostic is to measure the magnetic pitch angle distribution, or the ratio of poloidal to toroidal field strength, B_p/B_t. In the absence of radial electric fields, the polarization angles of the σ or π components are directly related to B_p/B_t through

$$\tan(\gamma_p) = \frac{B_p}{B_t}\frac{\cos(\alpha + \Omega)}{\sin(\alpha)}, \tag{6}$$

where γ_p is the polarization angle relative to the $B_p = 0$ reference, α is the angle between the toroidal field and the beam direction, Ω is the angle between the toroidal field and the view direction, and all three vectors are in the same plane. However, this relation is valid only when the upper levels of σ and π components are in statistical distribution. In Figure 13, we show our calculated polarization angle of the σ_0 component as a function of B_p/B_t for the beam into gas model at a density of 10^{13} cm^{-3}, and for beam into plasma models at densities of 10^{13} and 10^{14} cm^{-3}. It is seen that the beam into plasma relation for the density of 10^{14} cm^{-3} agrees with the geometrical prediction very well,
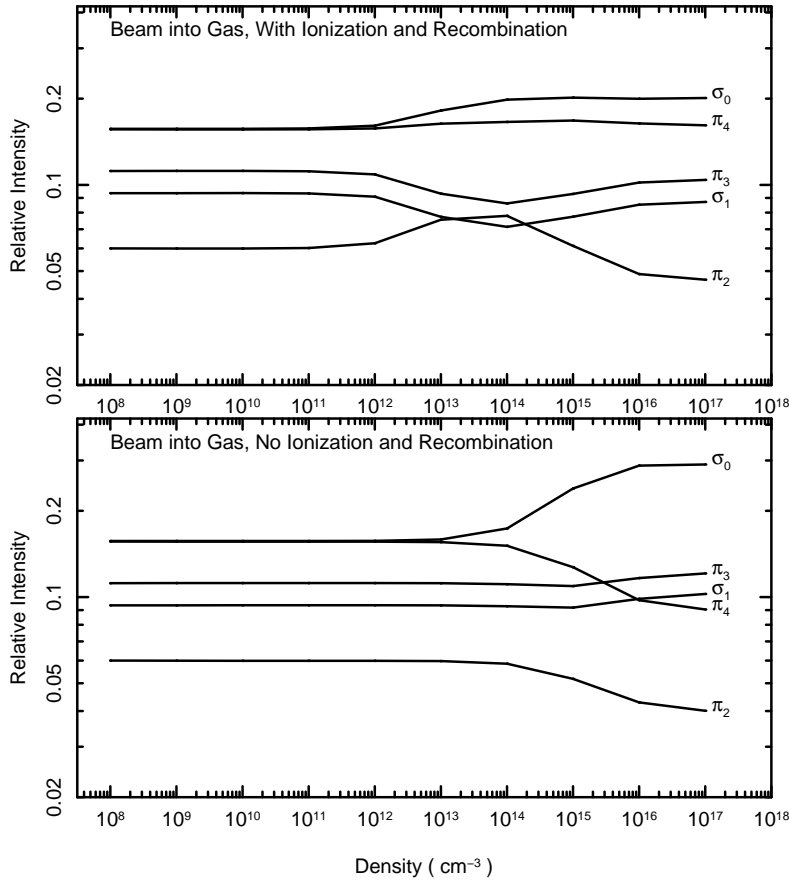
Figure 12. Relative intensities of σ and π components as functions of plasma density for beam into gas models.

the agreement for the density of 10^{13} cm^{-3} beam into plasma case is slightly worse, and the beam into gas relation is significantly different from the geometric prediction.

Another method of determining the B_p/B_t ratio is to measure the I_π/I_σ intensity ratio with an appropriate view direction. The π and σ intensities have angular distribution factors of $\sin^2 \Phi$ and $\frac{1}{2}(1+\cos^2 \Phi)$, respectively, where Φ is the angle between the view direction and the electric field. However, for view directions that are in the $\vec{v}$-$\vec{B}_t$ plane, Φ is nearly 90°, and the intensity ratios are not sensitive to the change in B_p/B_t. The measurement is most sensitive when Φ is close to 30°. One must also take into account the fact that the intensity ratios depend on whether the upper states are in statistical distribution. Fortunately, there exists two pair of lines, $\pi_{\pm3}/\sigma_{\pm1}$, whose ratios are largely independent of the upper level populations, which can be seen from the density independence of these ratios in Figure 11 and 12. This is due to the fact that $\pi_{\pm3}$ and $\sigma_{\pm1}$ mainly arise from a same set of upper levels. In Figure 14, we show our calculated $I(\pi_3)/I(\sigma_1)$ as a function of B_p/B_t for a particular view direction, which has a polar angle of 60° around $\vec{B}_t$, and an azimuth angle of 330° around $\vec{v} \times \vec{B}_t$. The relations for beam into plasma and gas models at a density of 10^{14} cm^{-3} and the geometric prediction based on the angular distribution factors of linearly polarized light
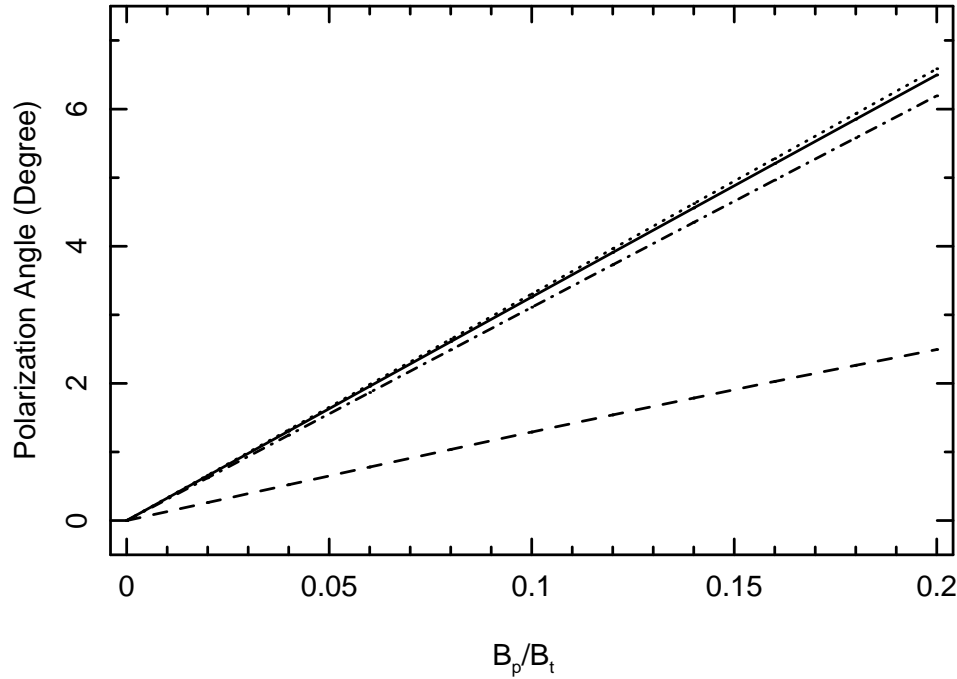
Figure 13. Polarization angle of the σ_0 component as a function of B_p/B_t. The solid line is calculated from the density matrices of individual Stark-Zeeman components for the beam into plasma model at a density of 10^{14} cm^{-3}, the dot-dashed lines are for beam into plasma model at a density of 10^{13} cm^{-3}, the dashed line is for the beam into gas model at a density of 10^{13} cm^{-3}, and the dotted line is the geometric prediction.

all agree with each other very well. Clearly, one can take advantage of this independence on the upper level populations to perform beam into gas calibration for such instruments.

5. Comparison with DIII-D Measurements

The DIII-D tokamak has four MSE diagnostic arrays from different view directions as shown in Figure 15. A conventional polarimetry system is used to detect polarization signals. The system employs a pair of photo-elastic modulators (PEM), which produces signals at two frequencies. One corresponds to $\sin 2\gamma_p$, and the other to $\cos 2\gamma_p$. In order to carry out actual measurements in a plasma using these two signals, the MSE diagnostic must be properly calibrated. Beam in gas measurements have been used mainly to determine the pitch angle offset. One of the difficulties encountered in the beam into gas calibration is that the observed Balmer α spectrum are different from those obtained in plasma shots. The DIII-D MSE system measures the polarization angles of the σ components. However, due to the finite bandwidth of the interference filters used in the system, the measured signal is contaminated by some fraction of the π components. Therefore, the larger ratio of π/σ for the beam into gas case represents a serious problem in the calibration procedure. In practice, the π/σ ratio is empirically increased by a factor of two in analyzing the beam into gas polarization spectrum. The atomic models presented in this paper provide the physical foundation for such empirical
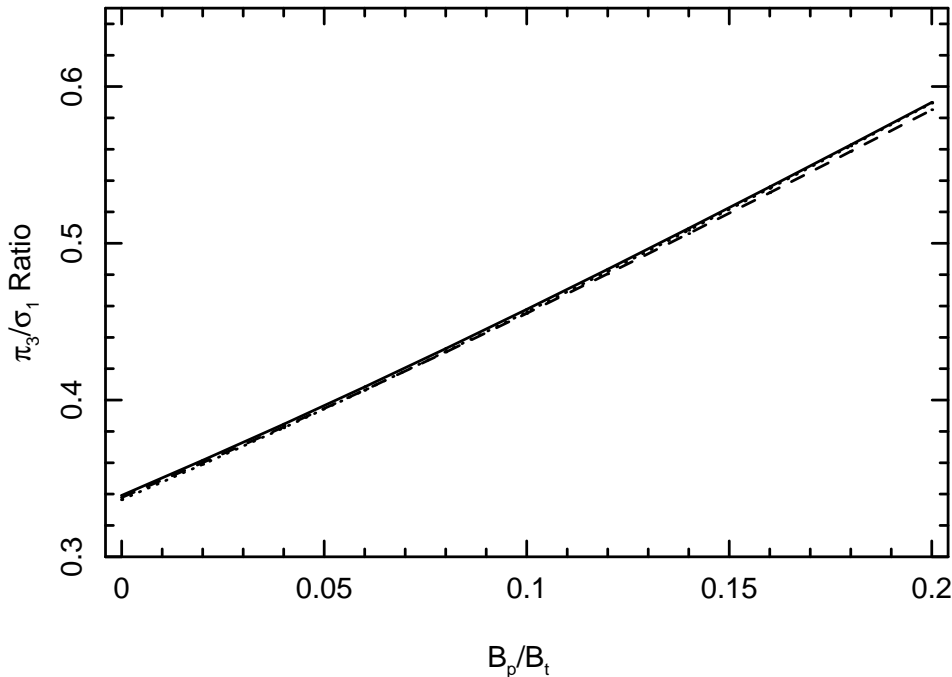
Figure 14. $I(\pi_3)/I(\sigma_1)$ as a function of B_p/B_t. The solid line is calculated from the density matrices of individual Stark-Zeeman components for the beam into plasma model at a density of 10^{14} cm^{-3}, the dashed line is for the beam into gas model, and the dotted line is the geometric prediction.

adjustments. However, our improved models for beam into gas measurements do not fit the experimetal spectra perfectly either, and here we quantify the differences in the calculated and measured intensity ratios of π and σ components. It is worth noting that the mixing of π and σ components may not be as large of a problem in future devices, such as ITER, where larger Stark electric fields are expected, resulting larger separations between different Stark components.

The polarization spectra from the MSE system on DIII-D are obtained with the so-called filter-scan technique, in which the interference filters are tilted to shift the center wavelengths to shorter values. The signal, proportional to $I_\sigma - I_\pi$, is recorded as a function of the filter tilt angle, giving the polarization spectrum broadened by the filter bandwidth and beam divergence. Figure 16 shows the measured spectra of beam into plasma and gas shots for the MSE channel 6 taken at a toroidal field of 2.1 T. The observed signal at the filter tilt angle θ is modeled as

$$I(\theta) = \sum_i x_p I_i G(\lambda(\theta) - \lambda_i), \tag{7}$$

where λ_i and I_i are the wavelengths and intensities of individual Stark-Zeeman components with negative intensities for lines from the π group. x_p is a multiplying factor to adjust the calculated intensities of the π components. Due to the limited spectral resolution and low statistical quality of the filter-scan data, we do not attempt to adjust the intensities of individual π lines, but assign a single multiplying factor for
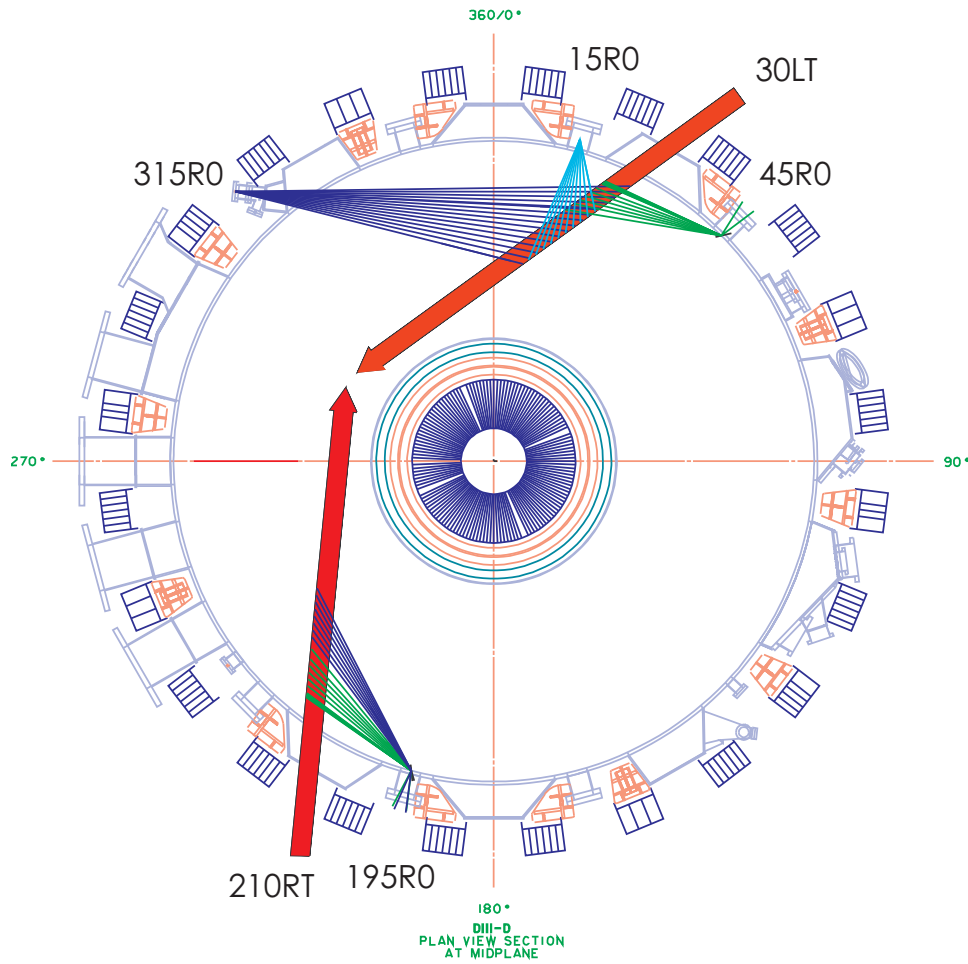
Figure 15. MSE diagnostic arrays at the DIII-D tokamak.

all lines in the group. $\lambda(\theta)$ is the center wavelength of the filter at a tilt angle of θ, which is approximated as

$$\lambda(\theta) = \lambda(0) - a(x - x_0)^2, \tag{8}$$

where x is a digitized voltage reading proportional to θ. The filter transmission profile is modeled by a Gaussian function with the FWHM, w, determined as

$$w^2 = [w_0 g(\lambda)]^2 + w_d^2, \tag{9}$$

where w_0 is the FWHM of the filters at zero tilt angle, $g(\lambda)$ models the dependence of the FWHM on the filter center wavelength λ, and w_d is the FWHM of the Dopler broadening due to the beam and view direction divergence. The integrated transmission efficiency may also decrease as the filters are tilted. In the analyses of the filter-scan data, the wavelength dependences of the FWHM and the integrated transmission are interpolated from the measured transmission profiles at several tilt angles. The Dopler broadening, w_d, is fixed at 1.4 Å for all channels, which is chosen to be consistent with the spectroscopic measurement on a different neutral beam as discussed later in this section. This value for w_d also makes the theoretical predictions of the beam into plasma filter-scan agree with the observations.

The beam into gas model is calculated at a density of 1.6×10^{13} cm^{-3} corresponding to a pressure of 0.5 mTorr. The beam into plasma model is calcualted at an electron density of 5×10^{13} cm^{-3} and a temperature of 4 keV. Both spectra are jointly fit, so that the filter parameters, a and $\lambda(0)$ are the same for the two measurements. The best fit models are compared with the measurements in the top and bottom panels of Figure 16. The beam into gas measurement is also fit with a plasma model, and the result is shown in the middle panel of Figure 16. It is seen that the fit to the beam into plasma measurement agrees with the data very well. The adjustment factor to the π intensities is close to unity. The fit to the beam into gas measurement is of considerably lower quality. If the plasma model is used in the fit, the adjustment factor to the π intensities is 2.02, and when the gas model is used, it is 1.59. Therefore, the present beam into gas model improves the fit, but do not yet predict the measured intensity ratios perfectly.

To further investigate the discrepancies between the beam into gas measurements and models, we have analyzed a beam into gas shot taken at a different time for 11 MSE channels. The adjustment factors for the π intensities exhibit significant channel-to-channel variation as shown in Figure 17. The adjustment factors from the fits that use the plasma model are typically 30% larger than the gas model fits, which reflects the larger calculated π intensities in the gas models. The derived factors for channel 6 and 35 are particularly large as compared with other channels. Because the beam into plasma measurement on the same channel 6 agrees with the theory reasonably well, and the beam into gas measurement taken at a different time requires a different adjustment factor, it appears that the polarization spectra are contaminated by unknown channel and time dependent light sources in the beam into gas measurements. This conclusion is also supported by the fact that many other MSE channels in the same shot display spurious peaks in the π components as shown in Figure 18. In order to use the beam into gas measurement as an effective calibration procedure, such channel and time dependent light contaminations must be quantified by detailed analyses of filter-scan data or simultaneous spectroscopic observations, such as those obtained on the B-Stark spectrometer discussed below.

As metioned in the previous section, another potential method for measuring the pitch angle is to use the π/σ intensity ratios observed in appropriate directions. Unlike the MSE polarimetry, this method is insensitive to the polarization changes, but sensitive to the polarization dependent transmission of the spectrometer system. Such dependences can be easily calibrated using beam into gas measurements, especially when the intensities of $\pi_{\pm 3}$ and $\sigma_{\pm 1}$ can be individually measured, as their ratios do not depend on the assumption of upper state statistical populations. Such a diagnostic system, called B-Stark, has been designed at the DIII-D, and preliminary data taken for both beam into gas and plasma shots. The viewing geometry of this system is shown in Figure 19. The angle between the neutral beam and the toroidal direciton is 52.7°, and the view chord is 31.4° off the mid-plane. The beam was operated at 74.5 keV for the full energy component. The toroidal magnetic field strength was close to 1.9 T
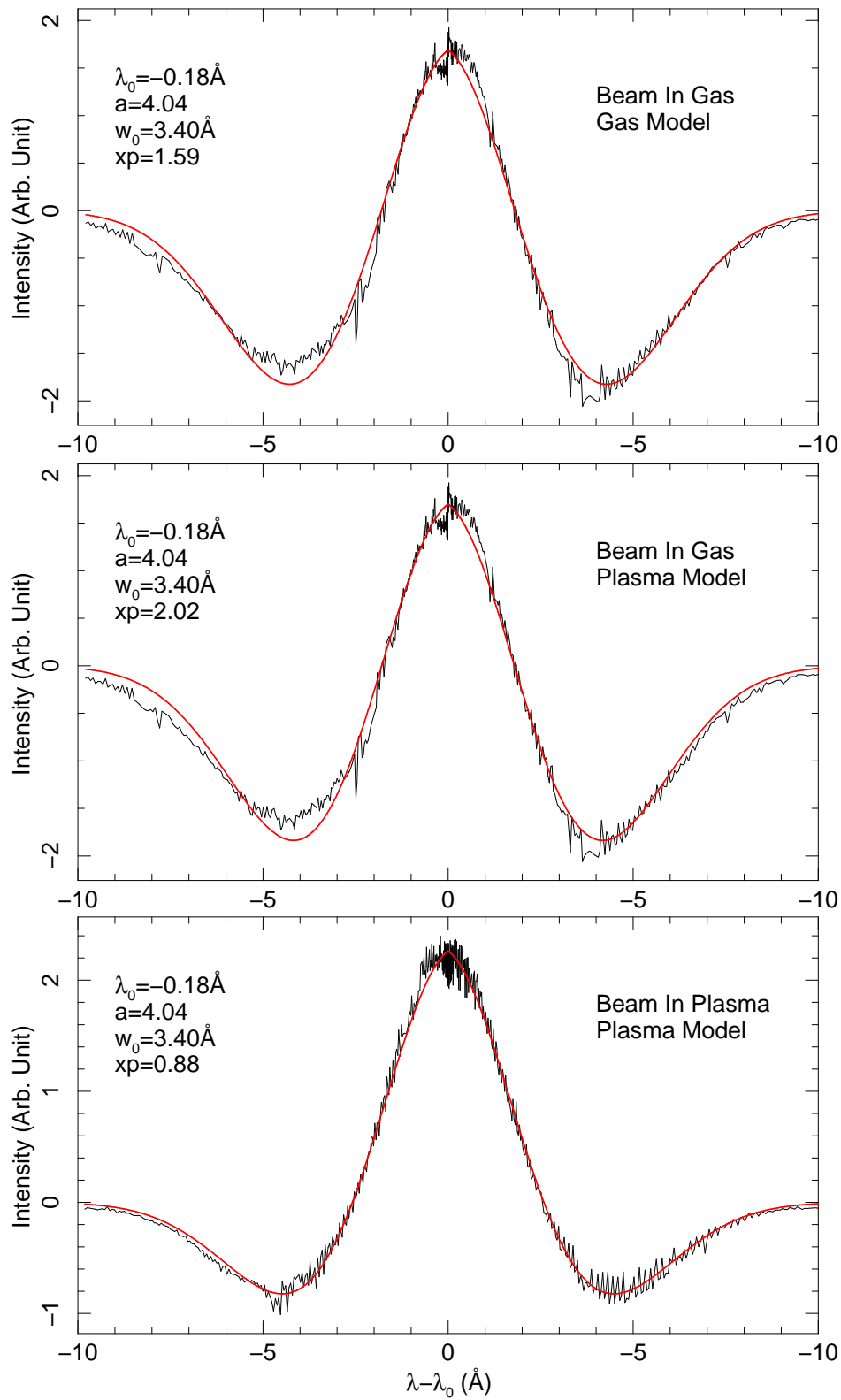
Figure 16. MSE filter-scan polarization spectra measured at the DIII-D tokamak in both beam into gas and plasma shots for channel 6 and comparison with the present calculations.
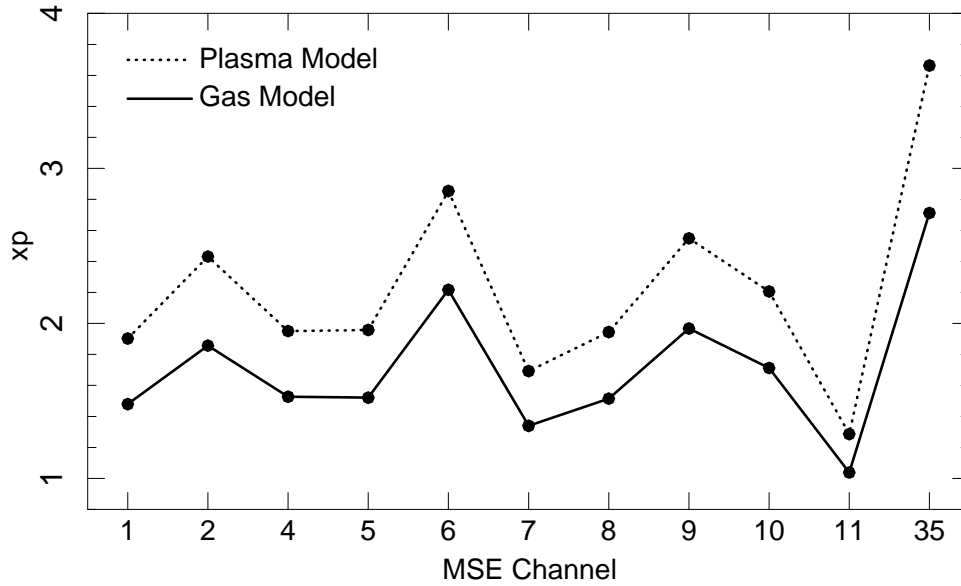
Figure 17. Adjustment factors for the π intensities in the beam into gas fit for 11 MSE channels with plasma and gas models.
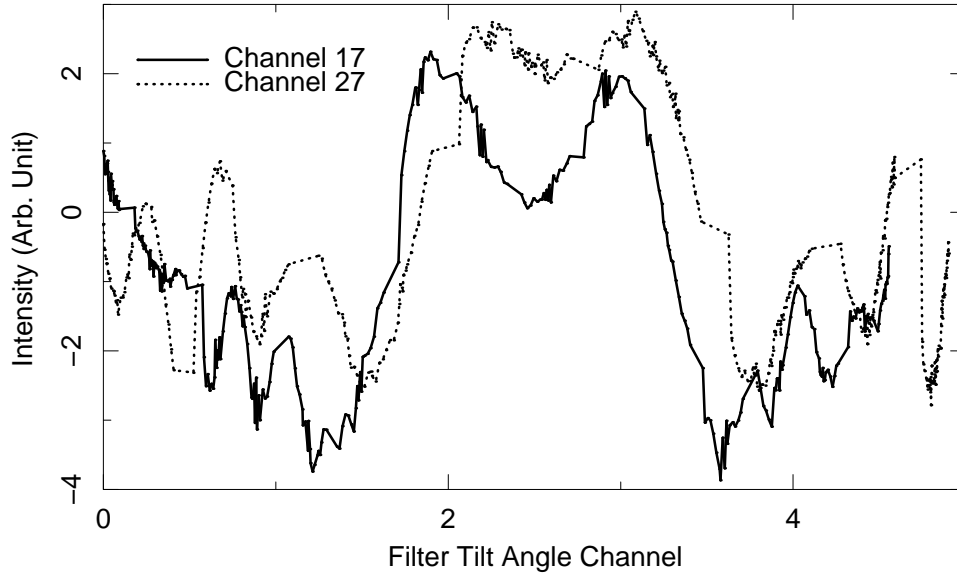

Figure 18. Filter-scan polarization spectra of 2 MSE channels with spurious peaks for the beam into gas measurement.

for both beam into gas and plasma measurements. We calculated the intensities and polarization states of all individual Stark-Zeeman components for both conditions in this specific geometry. The results for the beam into gas case are then folded through a parametrized spectrometer response to fit the observed data. The complete spectral model can be described as

$$I(\lambda) = \sum_e \sum_i a^e S_i^e L^e(\lambda - \lambda_i^e) + B(\lambda), \tag{10}$$

where $B(\lambda)$ is a smooth background, $e = 1$, $1/2$, and $1/3$ represent full, half, and third
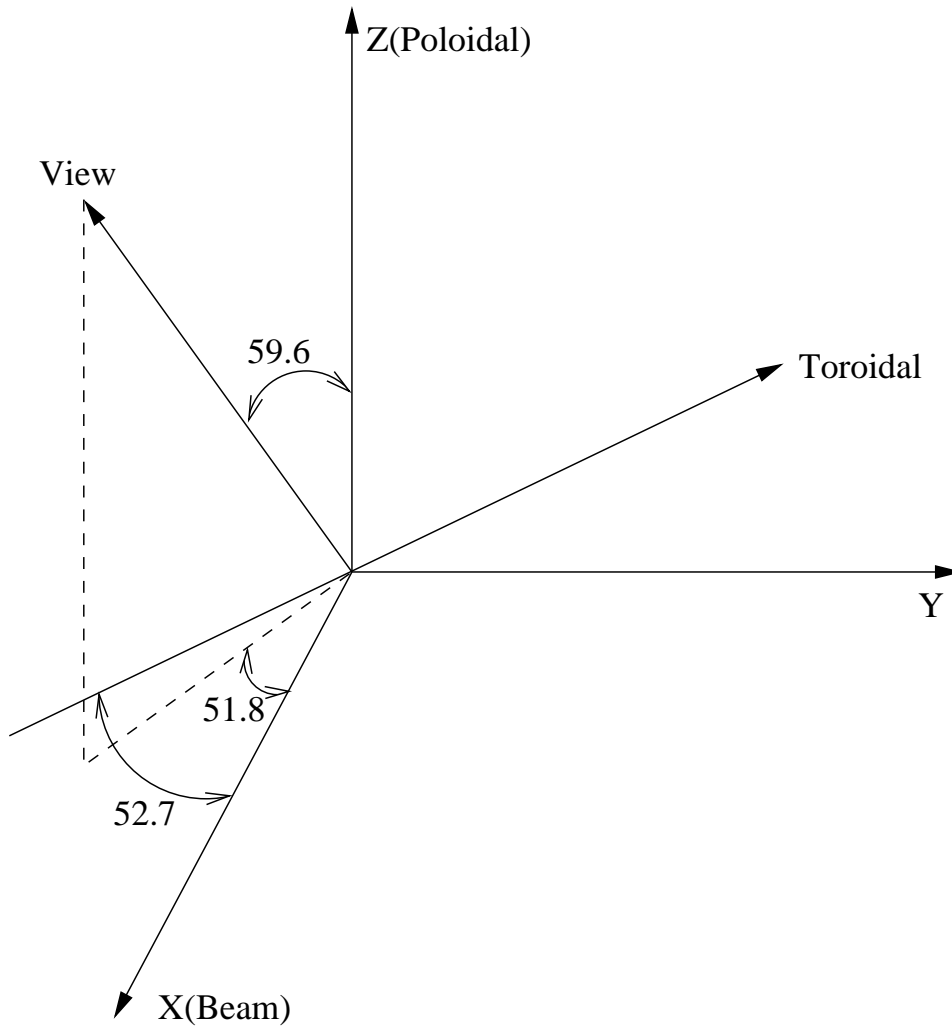
Figure 19. Viewing geometry of the B-Stark system at the DIII-D tokamak for π/σ intensity ratio measurements.

energy components of the neutral beam, a^e denotes the relative fraction of each energy component, λ_i^e and S_i^e are the wavelength and intensity of an individual Stark-Zeeman line for the beam energy component e. The wavelengths take into account proper Dopler shifts. The line profile $L^e(\lambda)$ is described by a Gaussian function with the FWHM, w, given by

$$w^2 = w_0^2 + ew_1^2, \tag{11}$$

where w_0 represents the instrument width common to all energy components, and w_1 gives the width caused by the beam and view direction divergence.

To calculate the intensities of Stark-Zeeman lines, we assume that the specctrometer acts as a partial linear polarizer with a polarization efficiency of r and the polarization axis resides within the plane of the photon direction and the poloidal direction. Therefore S_i can be written as

$$S_i = x_m(I_i + rQ_i \cos 2\theta - rU_i \sin 2\theta)\frac{W_i(\Phi)}{W_i(\Phi_0)}, \tag{12}$$

Table 2. Spectral fit parameters for the beam into gas calibration models "111", "101", and "000".

Model	w_0 (Å)	w_1 (Å)	r	x_1	x_2	x_4
111	0.4206	1.7834	0.2482	1.0000	1.0000	1.0000
101	0.5007	1.3609	0.2147	1.0000	1.7648	1.0000
000	0.5091	1.4421	0.1331	0.9697	2.0529	1.2863

where $W_i(\Phi)$ is the angular distribution factor with Φ being the angle between the view direction and the electric field direction, which depends on the magnetic pitch angle for a given viewing geometry, and takes the value of Φ_0 for $\gamma_p = 0$. θ is the angle between the spectrometer polarization axis and the x-axis of the coordinate system in which the Stokes parameters, I_i, Q_i, and U_i, are calculated, which lies in the plane defined by the photon direction and the electric field direction. In principle, the $W_i(\Phi)$ factors for each Stark-Zeeman component can be modeled. However, as Figure 14 illustrates, the detailed calculations using the Stokes parameters agree well with the simple geometric prediction assuming pure linear polarizatoins. Therefore, we adopt $W_i(\Phi) = \sin^2 \Phi$ and $(1 + \cos^2 \Phi)/2$, for π and σ Stark components, respectively. Unlike in the analyses of the filter-scan spectra, we assign empirical adjusting factors x_m for individual Stark components, with $m = 0$–4, representing σ_0, $\sigma_{\pm 1}$, $\pi_{\pm 2}$, $\pi_{\pm 3}$, and $\pi_{\pm 4}$, respectively. These parameters can be individually constrained since the B-Stark spectra are of higher statistical quality and better spectral resolution than the filter-scan data of the MSE polarimetry system. Because $\sigma_{\pm 1}$ and $\pi_{\pm 3}$ mainly arise from the same set of upper levels, x_1 and x_3 are constrained to be the same. x_0 is absorbed in the overall normalization of the model, and is therefore fixed at unity in the spectral fit.

With the calculated wavelengths and Stokes parameters of all Stark-Zeeman components, the spectral model described above is used to fit the observed data for both beam into gas and plasma shots. The beam into gas measurement was taken at a density of $\sim 2 \times 10^{12}$ cm^{-3}. We first fit the spectrum with three differerent procedures depending on whether x_1, x_2 and x_4 are varied as free parameters or fixed at unity. In model "111", all three multiplying factors are fixed at unity, in model "101", only x_2 is allowed to vary, and in model "000", all three are free parameters. The poloidal field is zero in the beam into gas shot, and we neglect radial electric fields. Therefore the angular distribution factors $W_i(\Phi)/W_i(\Phi_0)$ are all unity. The derived parameters of the spectral models are shown in Table 2. The comparison of model fits and the observed spectrum are shown in Figure 20. It is clear that the model "111" fit is unacceptable. It underestimates the intensities of $\pi_{\pm 2}$ relative to other π components. Varying x_2 in model "101" improves the fit considerably. However, there seems to be slight mismatch in the $\sigma_{\pm 1}/\sigma_0$ and $\pi_{\pm 4}/\pi_{\pm 3}$ ratios in the calculation as well. The model "000" best reproduces the observed spectrum. In this best-fit model, the calculated intensities of $\sigma_{\pm 1}$ and $\pi_{\pm 3}$ relative to σ_0 are multiplied by a factor of 0.97, those of $\pi_{\pm 2}$ is enhanced by a factor of 2.05, and those of $\pi_{\pm 4}$ are enhanced by a factor 1.29. These adjustment factors represent the uncertainties in our atomic model. Becasue $\pi_{\pm 2}$ is the weakest in
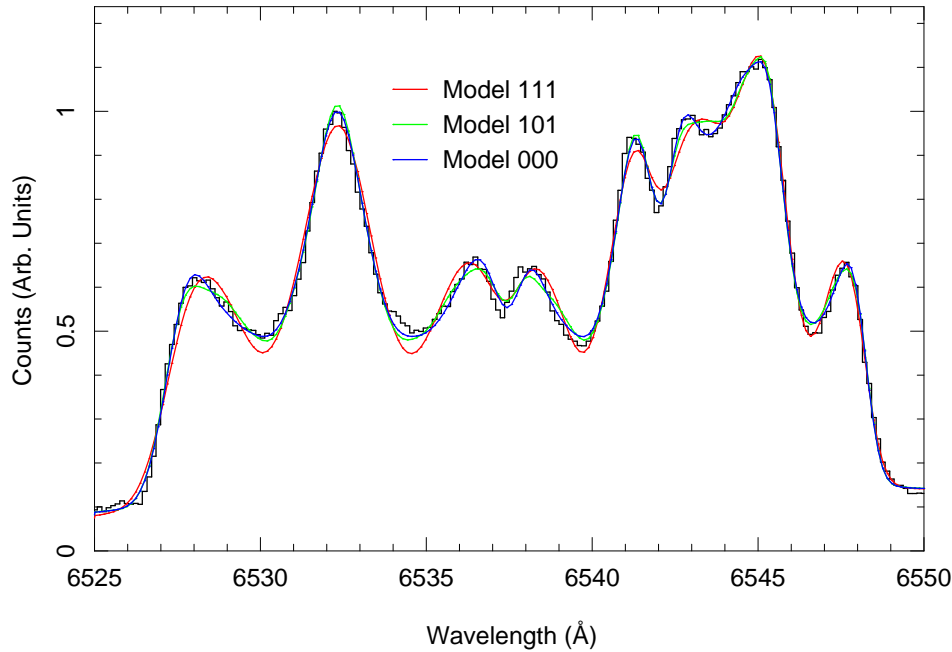
Figure 20. The measured spectrum and model fits for the beam in gas shot. The models "111", "101", and "000" are described in the text.

the π group, the overall enhancement factor for the π components is consistent with the lowest adjustment factors derived in the MSE filter-scan data, such as those for channels 1, 4, 5, 7 and 11. The higher values observed in the filter-scan data, such as those for channels 6, 9, and 35, are not consistent with the B-Stark spectrum, indicating possible light polution in those MSE channels.

The dervied value for the spectrometer polarization coefficient is 0.1329 in the model "000", or an efficiency ratio of 1.31 for the two polarization directions. The polarization coefficients derived from models "111" and "101" are considerably larger, at 0.2482 and 0.2147, respectively. Because the main constraint for this parameter in the mdoel "000" is the observed $\pi_{\pm3}/\sigma_{\pm1}$ ratio , which do not depend sensitively on the upper state population distributions, the value derived in model "000" is expected to be most reliable. If the spectral resolution can be increased by reducing the Dopler broadening, the accuracy of determining this parameter may be improved considerably.

For the beam into plasma shot, we divide the observed spectra into 10 ms bins for a total time of 1 s, during which the neutral beam was active. The time evolution of the plasma density and electron temperature are shown in Figure 21, and those of the toroidal and poloidal field strengths are given in Figure 22. The poloidal field strengths are obtained from the MSE polarimetry measurements. The plasma density is relatively low, especially in the beginning of the neutral beam activation. With such conditions, deviations to the statistical distribution for the $n = 3$ level populations are expected. Figure 11 indicates that this is the regime where the relative intensities of σ and π components are sensitive functions of the plasma density. Therefore, theoretical models employed in the spectral fit must be calculated with the measured plasma densities.
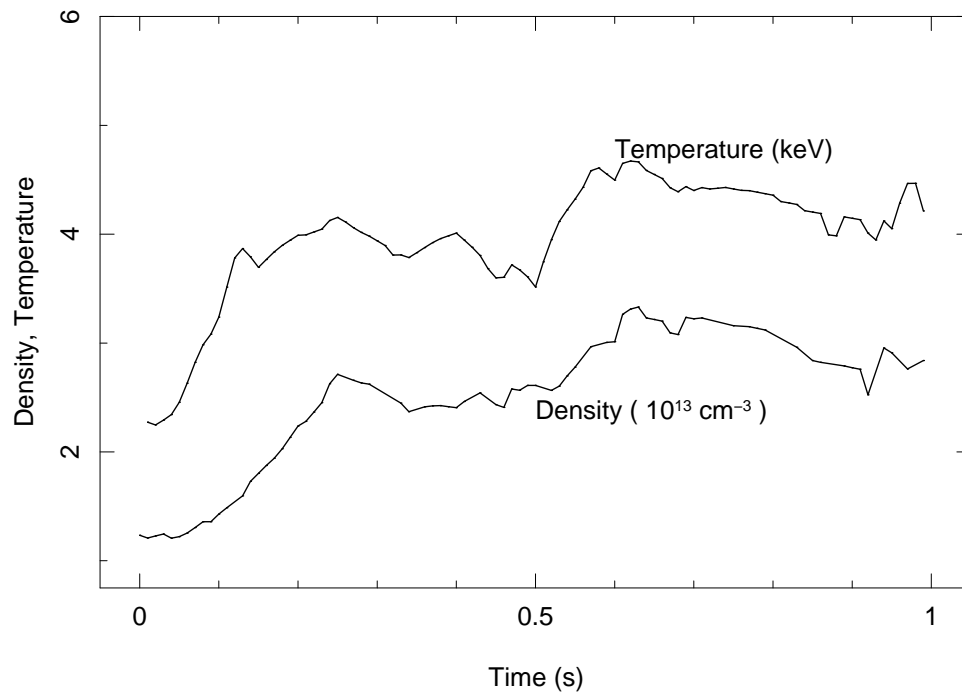
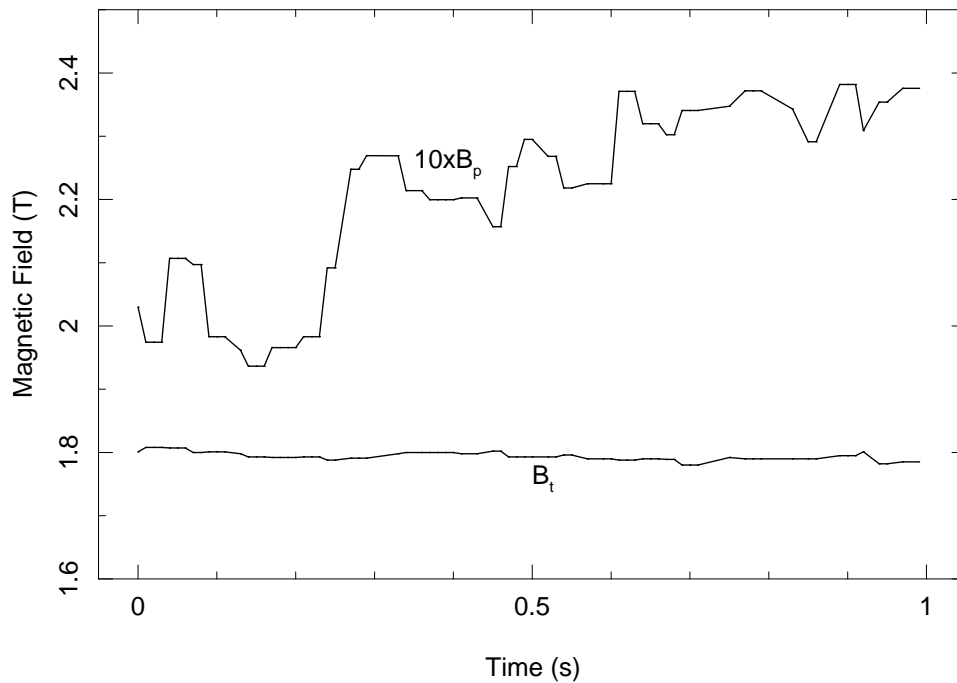**Figure 21.** The time evolution of the plasma density and temperature.

Figure 22. The time evolution of the toroidal and poloidal field strengths.

The exact values of electron temperatures are less important, as the cross sections are dominated by beam-ion collisions, and the relative collision velocities are determined by the beam energy, instead of the temperature. Therefore, we have adopted an electron temperature of 4 keV for all our beam into plasma models.
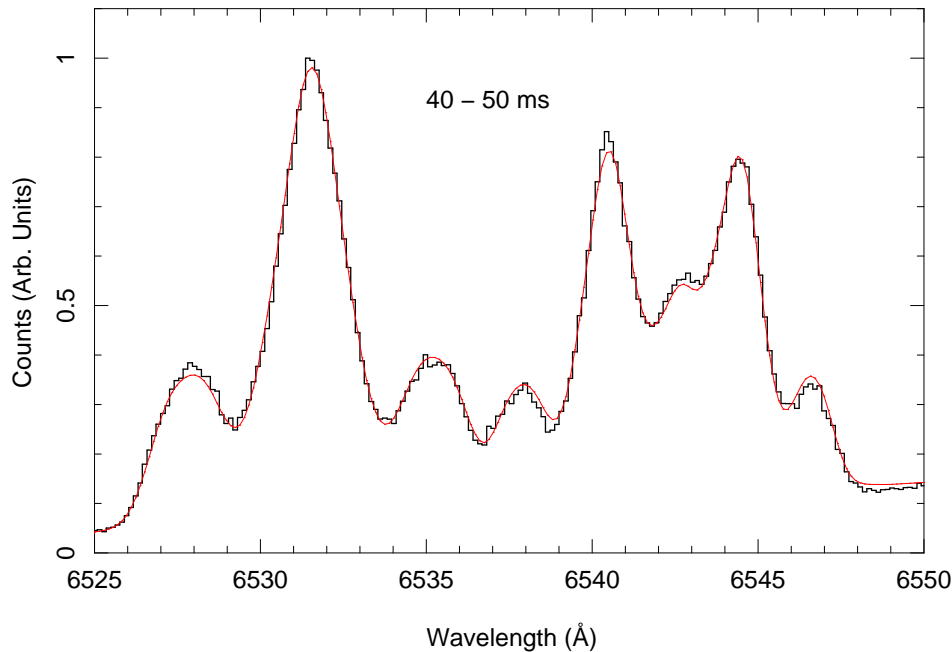
Figure 23. The measured spectrum and model fit of the beam in plasma shot during the time slice of 40–50 ms after the neutral beam activation.

Spectrum for each time bin is analyzed individually. In spectral fitting, the spectrometer polarization efficiency, r, is fixed at the value derived from the beam into gas calibration spectrum. Because theoretical models for beam into plasma are expected to be more reliable than the beam into gas models, we fix all x_m parameters at unity in the analyses. An additional free parameter in the beam in plasma model fits is the magnetic pitch angle due to the non-vanishing poloidal field. An example of the spectral fitting is shown in Figure 23 for the time slice of 40–50 ms after the neutral beam activation. Spectral fits are performed using three different values of the spectrometer polarization efficiency parameter, r, dervied from beam into gas models, "111", "101", and "000", respectively. The quality of the fit to the beam into plasma spectra using all three values are similar. Different r values simply result in different values for γ_p, and therefore B_p/B_t. The time evolution of the derived B_p/B_t are shown in Figure 24. It is clear that the r value derived from the beam into gas model "000" results in B_p/B_t measurements that agree very well with those derived from the MSE polarimetry system.

It is interesting to note that this good agreement is obtained only if the measured plasma density is used in the spectral models for the beam into plasma spectra. Figure 24 also shows the derived B_p/B_t for a model that assumes statistical population distribution. It is seen that the resulting B_p/B_t values are too small, and the considerable variation between 0 and 250 ms is more pronounced than that measured from the MSE polarimetry system. This variation is directely related to the rapid plasma density change from $\sim 1 \times 10^{13}$ to 3×10^{13} cm^{-3} during the first 250 ms. Using measured densities in the theoretical models reduces this variation, leading to good agreements
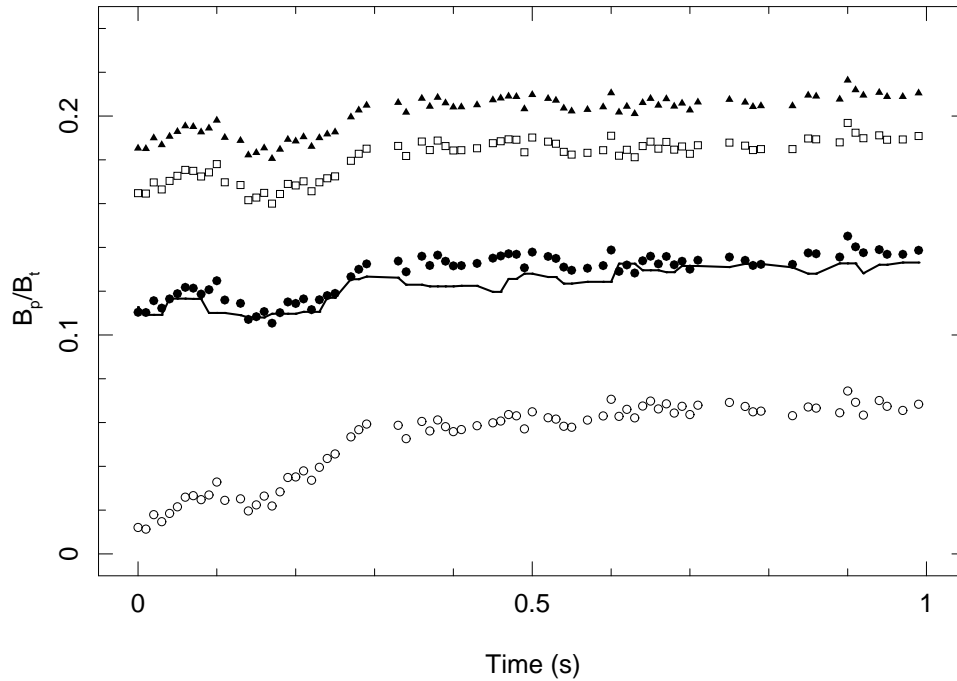
Figure 24. The time evolution of the B_p/B_t ratio. The solid line are determined from the MSE polarimetry system. The filled circles are derived from the beam into plasma spectral fit with the beam into gas calibration model "000" and density dependent beam into plasma models, the filled triangles are results obtained with the beam into gas calibration model "111", the open squares correspond to the beam into gas calibration model "101", and the open circles are the results using the beam into gas calibration model "000", but the beam into plasma models assume statistical population distribution for the $n = 3$ states.

with the B_p/B_t values derived from the polarimetry system.

6. Conclusions

Detailed atomic models are constructed for the MSE diagnostic. Various collisional cross sections are calculated in the first Born approximation. The intensities and polarization states of individual Stark-Zeeman components of the Balmer α line are investigated in detail. Collisional radiative model calculations indicate that for typical beam into gas measurements at densities below a few $\times 10^{13}$ cm^{-3}, the populations of $n = 3$ states are far from statistical distribtuion, leading to much larger π/σ line ratios than those observed in the beam into plasma measurements. Statistical population distribution is a reasonable approximation for beam into plasma shots at densities above 5×10^{13} cm^{-3}. The deviation from the statistical distribution is appreciable at lower densities.

Our beam into gas models provide a qualitative explanation for the observed π/σ intensity ratios. However, empirical adjustment factors ranging from 1.0–2.0 must still be applied to the σ and π intensities to bring the model predictions into full agreement with the observed spectra. Nevertheless, if high quality filter-scan or spectroscopic

data are available, such discrepancies are easily quantifiable and their effects on the calibration results may be minimized. The fact that $\pi_{\pm 3}/\sigma_{\pm 1}$ ratios are insensitive to the upper level populations is particularly useful in such calibration processes. We have successfully used this feature to calibrate the B-Stark spectrometer on DIII-D with beam into gas measurements, and derived the magnetic pitch angle values that are consistent with those obtained from the polarimetry system.

The analyses of filter-scan polarization spectra on the DIII-D MSE system indicate the existence of unknown channel and time dependent light contaminations in the beam into gas measurements. The source of such contaminations must be identified before the beam into gas measurement can be used as a reliable calibration method.

Acknowledgments

References

Belkić, D., Gayet, R., & Salin, A. 1984, Computer Physics Communications, 32, 385

Boileau, A., von Hellerman, M., Mandl, W., Summers, H. P., Weisen, H., & Zinoviev, A. 1989, Journal of Physics B Atomic Molecular Physics, 22, L145

Foley, E. L. & Levinton, F. M. 2006, Journal of Physics B Atomic Molecular Physics, 39, 443

Geddes, J., Hill, J., Yousif, F. B., & Gilbody, H. B. 1987, Journal of Physics B Atomic Molecular Physics, 20, 3833

Gillespie, G. H. & Inokuti, M. 1980, Phys. Rev. A, 22, 2430

Hill, J., Geddes, J., & Gilbody, H. B. 1980, Journal of Physics B Atomic Molecular Physics, 13, 951

Hughes, R. H., Petefish, H. M., & Kisner, H. 1972, Phys. Rev. A, 5, 2103

Inokuti, M. 1971, Reviews of Modern Physics, 43, 297

Levinton, F. M., Fonck, R. J., Gammel, G. M., Kaita, R., Kugel, H. W., Powell, E. T., & Roberts, D. W. 1989, Physical Review Letters, 63, 2060

Levy II, H. 1969, Physical Review, 187, 130

Mandl, W., Wolf, R. C., von Hellermann, M. G., & Summers, H. P. 1993, Plasma Physics and Controlled Fusion, 35, 1373

McKee, J. D. A., Geddes, J., & Gilbody, H. B. 1979, Journal of Physics B Atomic Molecular Physics, 12, 1701

Park, J. T., Aldag, J. E., George, J. M., & Peacher, L. L. 1976, Phys. Rev. A, 14, 608

Steffen, R. M. & Alder, K. 1975, in The Electronmagnetic Interaction in Nuclear Spectroscopy, ed. W. D. Hamilton (J. Wiley & Sons, New York), 505

Wróblewski, D., Burrell, K. H., Lao, L. L., Politzer, P., & West, W. P. 1990, Review of Scientific Instruments, 61, 3552